PAPER

Check for updates

Stretchable, self-healable, and adhesive ionogels formed *via* dual association of complex copolymers

Hyeonji Lee,† Min Su Kim,† Minha Lee, Seungjun Kim, Keun Hyung Lee ✶* and Myungwoong Kim ✶*

We report the fabrication of freestanding, stretchable, highly adhesive, ionically conductive, and self-healable ionogels consisting of an ionic liquid (IL) and two types of copolymers bearing hydrogen bonding acceptor and donor units: (i) poly[*tert*-butyl styrene-*b*-(4-hydroxystyrene-*r*-methyl acrylate)-*b*-*tert*-butyl styrene], and (ii) poly(2-vinyl pyridine-*r*-methyl acrylate). These copolymers yield an associative ionogel by forming micelles *via* IL-phobic interactions, and the micelles interact through hydrogen bonding between corona blocks, bridging by stretched block copolymer chains, or hydrogen bonding between the corona block and the additional pyridine-bearing copolymer chains. By tuning the molecular weights and compositions, we fabricated freestanding ionogels exhibiting outstanding mechanical properties, including a strain at break of $\approx 1000\%$, toughness of ≈ 3000 kJ m^{-3}, and Young's modulus of ≈ 300 kPa, along with an ionic conductivity of ≈ 0.5 mS cm^{-1}. The ionogel adheres strongly to various substrates—such as plastics, elastomers, glass, and metals—with a maximum adhesion stress of ≈ 1300 kPa under ambient conditions. It remains adhesive even in water and demonstrates a self-healing efficiency greater than 95%. When applied as a strain sensor, the ionogel exhibits a highly linear and reversible strain–resistance response, with a gauge factor of 1.9 over a strain range of 10–100%, showing negligible hysteresis, rapid recovery, and stable performance under cyclic loading. The sensor also demonstrates exceptional self-healing capability and long-term durability, fully restoring its electrical response after complete severing and maintaining consistent signal output under 50% strain for over 20 000 s, confirming its suitability for reliable soft sensing applications.

1. Introduction

The transformation of body movement into electrical signals has attracted increasing attention with the rising demand for wearable electronic device.[1] Such devices are enabled by strain sensors, which convert physical deformation into changes in electrical signals, such as resistivity. Therefore, the material used must be conductive, stretchable, mechanically robust, and chemically stable.[2] These criteria have been met by combining rubbery materials, such as Ecoflex and poly(dimethylsiloxane) (PDMS), with various ion-conductive materials, including hydrogels.[3,4] Recently, ionogels, three-dimensional polymer networks swollen with ionic liquids (ILs), have gained attention as promising candidate materials for strain sensors. This is due

to their electrochemical stability, excellent physical properties, and chemical safety, attributed to the nonvolatility of ILs.[5,6]

Although ionogels have demonstrated unique properties for strain-sensing applications, further improvements are necessary to meet additional target requirements.[7–9] The strain sensor should be freestanding while maintaining its shape to avoid damage during operation on a target substrate.[10] It must not only stretch effectively during intense body movements but also return to its original state with sufficient elasticity.[11] Additionally, it should adhere well to various surfaces, allowing firm attachment without the need for separate adhesives or tape, even under dynamic conditions and varying environments.[12] Since strain sensors are prone to damage during use, wearable sensors should also possess self-healing capabilities to recover their original state upon the application of external stimuli such as heat.[10,13]

In the literature, ionogel materials have been developed through either covalent or noncovalent crosslinking mechanisms.[7,14,15] Among these, the use of block copolymers (BCPs)

Department of Chemistry and Chemical Engineering, Inha University, Incheon 22212, Republic of Korea. E-mail: mkim233@inha.ac.kr, kh.lee@inha.ac.kr
† These authors contributed equally to this work.

to form ionogels *via* noncovalent crosslinking has attracted significant interest due to their simple and cost-effective fabrication, as well as their reusability by dissolving the ionogels in selected organic solvents followed by remolding.[16–18] Furthermore, the chemical design of BCPs for targeted applications enables the tailoring of ionogel physical and chemical properties by controlling the type, sequence, and molecular weight of the blocks, along with the incorporation of functional groups to impart specific features.[19] For example, polystyrene-*b*-poly-(ethylene oxide)-*b*-polystyrene (PS-*b*-PEO-*b*-PS) self-assembles in ILs due to the IL-phobic nature of the PS blocks, forming micellar clusters associated *via* bridging by triblock copolymer chains.[20,21] However, this bridging interaction did not impart sufficient mechanical strength to support freestanding ionogels. This limitation was addressed by shifting the association mechanism to inter-micellar hydrogen bonding. Diblock copolymers were subsequently designed with an IL-phobic block (PS or poly(*tert*-butyl styrene)) and a second block containing IL-interactive units along with hydrogen-bonding motifs such as acrylamide, acrylic acid, 4-hydroxystyrene, and 2-vinyl pyridine.[22] In addition, to impart self-healabilty into the iongel materials, the polymer network needs to be designed with the functionalities that can make dynamic formation of covalent bonds (*e.g.* dihydrazone formation,[23] Diels–Alder reaction,[24] and disulfide metathesis[25]) or non-covalent interactions (*e.g.* hydrogen bonding[26] and ion–dipole interaction,[27] and metal–ligand interaction[28]), with appropriate design of polymer networks that can enhance chain mobility and dynamic network rearrangement to promote efficient self-healing behaviors. Although these gel materials demonstrated favorable mechanical and electrochemical properties, achieving a multifunctional ionogel that simultaneously meets all of the aforementioned requirements remains a significant challenge.

Herein, to address this challenge, we design a material system capable of forming highly versatile ionogels that exhibit freestanding capability, mechanical robustness, stretchability, adhesiveness, and self-healability through the dual association of two types of complex copolymers. The system comprises two copolymer components: (i) the triblock copolymer poly-(*tert*-butyl styrene-*b*-(4-hydroxystyrene-*r*-methyl acrylate)-*b*-*tert*-butyl styrene) (PSHMS), and (ii) poly(2-vinyl pyridine-*r*-methyl acrylate) (PVM), combined with the IL, 1-ethyl-3-methyl-imidazolium bis(trifluoromethyl sulfonyl)imide ([EMIM][TFSI]). The IL-phobic poly(*tert*-butyl styrene) blocks assemble to form the cores of micellar clusters, while the triblock copolymer chains bridge these clusters to form a three-dimensional network. Additionally, a secondary association arises through hydrogen bonding between phenol groups in the middle block of PSHMS and pyridine groups in PVM. This dual association not only reinforces the polymer network in the IL but also introduces free hydrogen-bonding units, enabling both self-healing capability and effective adhesion. In this design, the effects of copolymer molecular weight and the composition of the two polymer components on mechanical, electrical, and self-healing properties were systematically investigated for

strain-sensor applications. Using the optimized composition, a self-healable strain sensor was fabricated and evaluated.

2. Experimental

2.1. Materials

All reagents were used without further purification unless otherwise noted. Carbon disulfide (>99.9%), sodium thiosulfate pentahydrate (>99.5%), 4,4′-azobis(4-cyanovaleric acid) (>98.0%), 1-dodecanethiol (>98%), 1-ethyl-3-methylimidazolium bis(trifluoromethylsulfonyl)imide ([EMIM][TFSI], ≥98%), methyl acrylate (MA; >99.0%), 4-methoxyphenol (99%), 4-hydroxybenzaldehyde (98%), 3,4-dihydro-2*H*-pyran (97%), pyridinium *p*-toluenesulfonate (PPTS; 98%), and methyltriphenylphosphonium bromide (PPh$_3$MeBr; 98%) were purchased from Sigma-Aldrich Co. Ltd. (Milwaukee, WI, USA). Iodine (>98.0%), 4-*tert*-butylstyrene (*t*BS; >90.0%), 2-vinyl pyridine (2VP; >97.0%), 1-(3-dimethylaminopropyl)-3-ethylcarbodiimide hydrochloride (EDC·HCl; >98.0%), and 4-dimethylaminopyridine (DMAP; >99.0%) were obtained from Tokyo Chemical Industry Co. Ltd (Tokyo, Japan). Ethyl acetate (EA; >99.0%), *n*-hexane (>95.0%), sodium sulfate (anhydrous, >99.0%), ammonium chloride (>99.0%), heptane (>98.0%), and Celite 545 were purchased from Daejung Chemical & Metals Co., Ltd (Siheung, Korea). Dichloromethane (DCM; 99.8%), hydrochloric acid (HCl; 35–37%), methanol (99.5%), potassium *tert*-butoxide (>98.0%), and diethyl ether (99%) were purchased from Samchun Chemicals Co. Ltd (Seoul, Korea). Sodium hydroxide (93.0%), sodium bicarbonate (99.5%), sodium chloride (99.0%), and tetrahydrofuran (THF; 99.5%) were obtained from Duksan Chemicals Co., Ltd (Ansan, Korea). Anisole (99%) was supplied by Thermo Fisher Scientific Co. Ltd. (Waltham, MA, USA). SYLGARD™ 184 silicone elastomer base and SYLGARD™ 184 silicone elastomer curing agent were purchased from Dow Chemicals (Midland, MI, USA). Poly(3,4-ethylenedioxythiophene):poly(styrene sulfonate) (PEDOT:PSS, Clevios PH1000) was purchased from Heraeus (Hanau, Germany). 2,2′-Azobis(2-methylpropionitrile) (AIBN) was obtained from Junsei Chemicals (Tokyo, Japan) and was recrystallized from methanol before use. The monomers, *i.e.*, *t*BS, MA, and 2VP, were purified by passing them through a neutral alumina column to remove inhibitors before polymerization. 4-(2-Tetrahydropyranyloxy)styrene (OTHPSt) was synthesized following a previously reported procedure.[29]

2.2. Synthesis of difunctional RAFT agent (CTA-EG)

A synthetic route for CTA-EG is depicted in Fig. S1. A 500 mL round-bottom flask was charged with potassium *tert*-butoxide (5.00 g, 45 mmol) dissolved in THF (69 mL), followed by the addition of heptane (182 mL), which rendered the reaction mixture opaque. The flask was sealed with a septum and purged with nitrogen for 20 min. The reaction mixture was maintained below 15 °C using an ice bath. Subsequently, 1-dodecanethiol (9.019 g, 45 mmol) was added dropwise, and the reaction mixture was stirred for 60 min. Upon formation of a white solid, carbon disulfide (3.39 g, 45 mmol) was added

slowly dropwise, and the mixture was stirred for an additional 90 min. Stirring was continued at room temperature for 5 h. Iodine (6.08 g, 24 mmol) was then added to the mixture, followed by stirring for 23 h. The reaction mixture was washed sequentially with aqueous sodium thiosulfate solution, brine, and deionized water. The organic layer was dried over sodium sulfate, and the solvent was removed using a rotary evaporator. The crude product was further dried under vacuum to yield bis(dodecylsulfanylthiocarbonyl) disulfide (BDSTD). The synthesized BDSTD (11.612 g, 21 mmol) and 4,4′-azobis(4-cyanopentanoic acid) (9.968 g, 36 mmol) were dissolved in ethyl acetate (159 mL) and refluxed at 75 °C for 35 h. The solution was cooled to room temperature and washed with deionized (DI) water, followed by drying of the organic layer over sodium sulfate. The solvent was removed using a rotary evaporator, affording a yellow solid. The crude product was recrystallized from heptane, followed by two successive recrystallizations from *n*-hexane, yielding 4-cyano-4-(phenylcarbonothioylthio)pentanoic acid (CDSTSP; 9.872 g, 24 mmol). Subsequently, ethylene glycol (0.19 g, 3 mmol) and CDSTSP (3.19 g, 8 mmol) were dissolved in DCM (16.5 mL) in a 50 mL round-bottom flask. To this mixture, EDC·HCl (2.83 g, 15 mmol) and DMAP (0.077 g, 0.6 mmol) were added, and the solution was stirred at room temperature for 21 h. After the reaction, the solution was concentrated using a rotary evaporator, and EA (100 mL) was added to dilute the solution. The mixture was washed sequentially with aqueous HCl (prepared by diluting 12 mL of HCl in 240 mL of DI water), aqueous NaHCO₃ solution (2.00 g in 240 mL of DI water), and brine. The organic layer was dried over sodium sulfate, stirred for 10 min, and filtered through a glass filter. The solvent was removed using a rotary evaporator, and the crude product was purified by column chromatography (eluent: EA/*n*-hexane, 2 : 8 v/v). Evaporation of the eluent yielded a yellow-orange product.

2.3. Synthesis of poly[*t*BS-*b*-(HS-*r*-MA)-*b*-*t*BS] (PSHMS)

Poly(OTHPSt-*r*-MA) (POM) was synthesized *via* RAFT polymerization by varying the molar ratio of RAFT agent to monomers (Table S1). As a representative procedure for synthesizing PSHMS-114k, OTHPSt (9.15 g, 45 mmol), MA (20.0 g, 0.23 mol), CTA-EG (0.051 g, 0.06 mmol), and AIBN (0.051 g, 0.30 mmol) were added to a 50 mL Schlenk flask equipped with a magnetic stir bar. Toluene (28 mL) was then added, and the mixture was degassed using three freeze–pump–thaw cycles. Polymerization was carried out at 60 °C for 4 h under stirring. The reaction was quenched by exposure to air, and the mixture was diluted with THF and precipitated into excess methanol. The resulting light-yellow solid was collected by vacuum filtration and dried under vacuum at 30 °C for 24 h, yielding the POM sample. For chain extension of the random copolymer (Table S2), a representative procedure as follows: POM (4.00 g), *t*BS (0.923 g, 6.0 mmol), and AIBN (0.0076 g, 0.05 mmol) were dissolved in anisole (16 mL) in a 50 mL Schlenk flask. The solution was degassed by three freeze–pump–thaw cycles and polymerized at 90 °C in an oil bath for 6 h. The reaction was quenched by exposure to air, diluted with THF, and precipitated into excess methanol.

The resulting white solid, poly[*t*BS-*b*-(OTHPSt-*r*-MA)-*b*-*t*BS] (PSOMS), was collected by vacuum filtration and dried under vacuum at 30 °C for 24 h. To deprotect the tetrahydropyranyl (THP) group of the OTHPSt unit in the middle block, PSOMS (5.0 g) was dissolved in a 1 : 1 mixture of THF (250 mL) and ethanol (250 mL). While stirring, a few drops of aqueous HCl (35–37%) were added. The reaction mixture was bubbled with argon and stirred at room temperature for 24 h under an argon atmosphere. After solvent removal using a rotary evaporator, the residue was dissolved in THF and precipitated into excess diethyl ether. The mixture was decanted, and the resulting white solid, PSHMS, was collected by centrifugation and dried under vacuum at 30 °C.

2.4. Synthesis of poly(2VP-*r*-MA) (PVM)

PVM was synthesized *via* RAFT polymerization by varying the molar ratio of RAFT agent to monomers to control the molecular weight (Table S1). As a typical procedure for PVM-87k, MA (15.0 g, 0.17 mol), 2VP (3.297 g, 31 mmol), CTA-EG (0.029 g, 0.03 mmol), and AIBN (0.029 g, 0.20 mmol) were added to a 50 mL Schlenk flask. The mixture was degassed *via* three freeze–pump–thaw cycles and then polymerized in an oil bath at 70 °C for 24 h. The reaction was quenched by exposure to air, diluted with THF, and precipitated into excess diethyl ether. The resulting yellow solid was collected by vacuum filtration and dried under vacuum at 50 °C for 30 h.

2.5. Fabrication of an ionogel with the copolymers

Desired amounts of PSHMS and PVM were dissolved in acetone at varying weight ratios of PSHMS to PVM (3 : 1, 2 : 1, 1 : 1, 1 : 2, and 1 : 3). [EMIM][TFSI] was then added to each solution at a copolymer to IL weight ratio of 4 : 6, followed by vigorous stirring. The homogeneous solution was poured into silicone mold of the desired shape and dimensions, and the solvent was slowly evaporated at 50 °C over 3 d, yielding ionogel sample.

2.6. Characterizations

¹H nuclear magnetic resonance (NMR) spectra were acquired using a JEOL JNM-ECZ400S 400 MHz spectrometer with CDCl₃ or acetone-d_6 as the solvent (14 scans; a relaxation delay: 10 s). Size-exclusion chromatography (SEC) was conducted on a Thermo Scientific Ultimate 3000 system equipped with three columns (Waters, Styragel HR5, HR4, and HR3), using THF as the mobile phase at a flow rate of 1 mL min⁻¹ and a temperature of 35 °C. Molecular weight data were obtained using a calibration curve constructed from ten polystyrene standards with M_n values of 1.2–2700 kg mol⁻¹ (Shodex). Fourier transform infrared (FT-IR) spectra were recorded in attenuated total reflectance (ATR) mode using a PerkinElmer Frontier spectrometer equipped with a UATR Diamond/ZnSe attachment by averaging at least 10 scans at a resolution of 4 cm⁻¹. Tensile tests were performed at room temperature on a universal testing machine (UTM; YEONJIN S-TECH) at an elongation rate of 0.1 mm s⁻¹. Young's modulus was estimated from the initial slope of the stress–strain curve in the strain region below 5%. Toughness was obtained by integrating the area under the

Fig. 2 (a) Synthetic scheme for poly[*t*BS-*b*-(HS-*r*-MA)-*b*-*t*BS] (PSHMS), (b–d) representative ^{1}H NMR spectra of the copolymer (PSHMS-114k) acquired at each step, and (e) SEC traces before (black) and after the chain extension with *t*BS (red).

Table 1 Chemical characteristics of the synthesized PSHMS and PVM

Entry	DP_{tBS}	$DP_{HS/2VP}$	DP_{MA}	F_{MA}	M_n (kg mol^{-1})	$Đ$
PSHMS-85k	131	180	325	0.644[a]	85.5	1.41
PSHMS-98k	119	222	401	0.640[a]	98.7	1.40
PSHMS-114k	167	242	437	0.656[a]	113	1.52
PSHMS-136k	145	316	571	0.592[a]	136	1.72
PVM-73k	—	237	555	0.701	73.9	1.82
PVM-87k	—	312	627	0.668	87.0	1.83
PVM-108k	—	367	809	0.688	108	2.09
PVM-139k	—	491	1015	0.674	139	2.24
PVM-151k	—	559	1077	0.658	151	1.99

[a] F_{MA} of the second block in the PSHMS.

block copolymerization. The compositions of MA and OTHPSt units (F_{MA} and F_{OTHPSt}) were tuned between 0.6–0.7 and 0.3–0.4, respectively, as determined by quantitative ^{1}H NMR analysis (Fig. 2b), based on integration of the methyl group signal of the MA unit at 3.0–3.8 ppm and the characteristic OTHPSt peaks at 5.2–5.5 ppm and 6.4–7.0 ppm. The macro-CTA was then successfully chain-extended with *t*BS *via* a second RAFT polymerization, as confirmed by a slight shift in the SEC peak (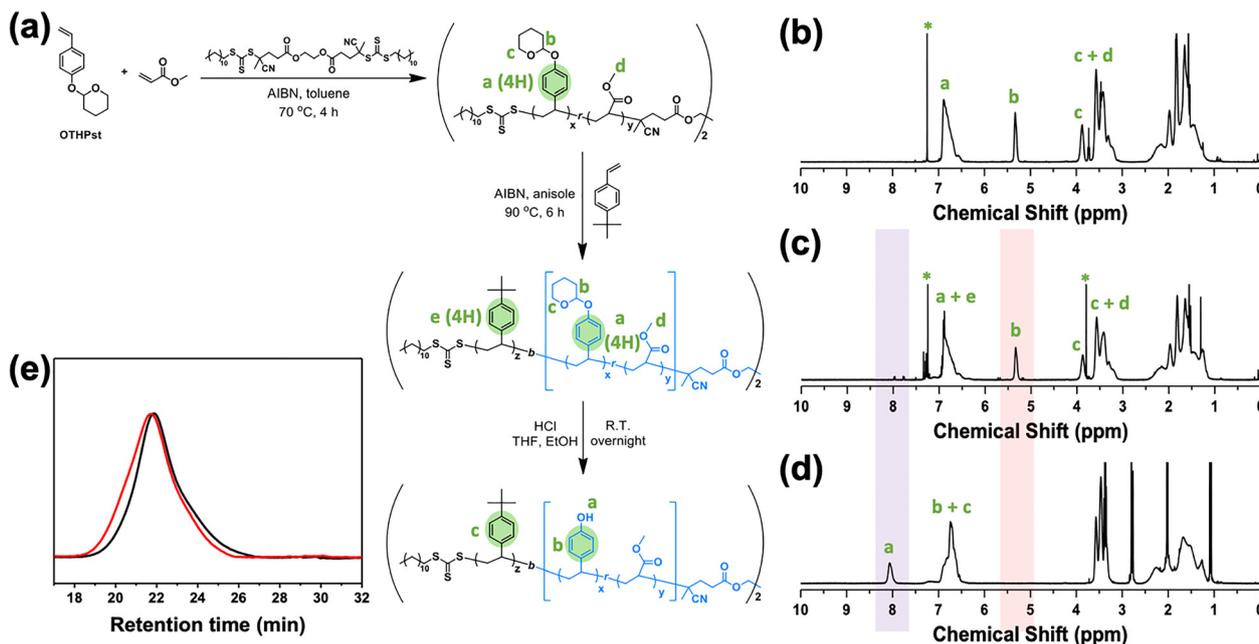Fig. 2e), indicating an increase in M_n of approximately 20 kg mol^{-1}. Subsequently, the OTHPSt units in PSOMS were deprotected *via* acid-catalyzed cleavage using a small amount of HCl.[29] In the ^{1}H NMR spectrum, the disappearance of the acetal proton signal at 5.2–5.5 ppm and the emergence of a new peak at 7.9–8.2 ppm, corresponding to the phenolic proton, confirmed successful deprotection (Fig. 2c and d). SEC and ^{1}H NMR spectra of additional PSHMS samples with different molecular weights are shown in Fig. S2. PVM with controlled M_n values ranging from 73 to 151 kg mol^{-1} was also synthesized *via* RAFT polymerization (Fig. 3a and b, Fig. S3). As confirmed by ^{1}H NMR spectroscopy,

the composition of MA and 2VP (F_{MA} and F_{2VP}, respectively) was determined by integrating the characteristic peaks of the methyl group in the MA unit (3.0–3.8 ppm) and the pyridine ring in the 2VP unit (8.1–8.6 ppm), showing variation in the ranges of 0.6–0.7 and 0.3–0.4, respectively (Fig. 3c).

3.2. Fabrication and chemical characterization of ionogels with the synthesized copolymers

To fabricate freestanding ionogels using the synthesized copolymers, PSHMS and PVM were dissolved in acetone at various weight ratios (w_{PSHMS} : w_{PVM} = 3 : 1, 2 : 1, 1 : 1, 1 : 2, and 1 : 3), and the resulting samples were designated as HV31, HV21, HV11, HV12, and HV13, respectively. [EMIM][TFSI] was then added to each solution at a copolymer-to-IL weight ratio of 4 : 6. Once a homogeneous solution was obtained, it was poured into a silicone mold and left to dry in an oven at 40 °C for at least 3 d, allowing acetone to evaporate and enabling polymer network formation *via* dual association between micellar clusters. The formation of hydrogen bonding was confirmed by FT-IR spectroscopy (Fig. 4). As the PSHMS content increased, a peak at 995 cm^{-1}, attributed to the bending mode of the aryl C–H group in the pyridine ring, shifted to a higher wavenumber, indicating strong hydrogen bonding between phenol and pyridyl groups.[32] Additionally, the broad peak at 3460 cm^{-1}, characteristic of phenolic O–H stretching in PSHMS,[33] decreased in intensity with increasing PVM content, suggesting interaction between the phenol groups in the HS units and the pyridine rings of the 2VP units.[34] Notably, the O–H peak did not disappear entirely, indicating that unbound phenol groups remained in the system. These free phenol groups likely play a pivotal role in imparting additional functions, such as adhesion and self-healing.
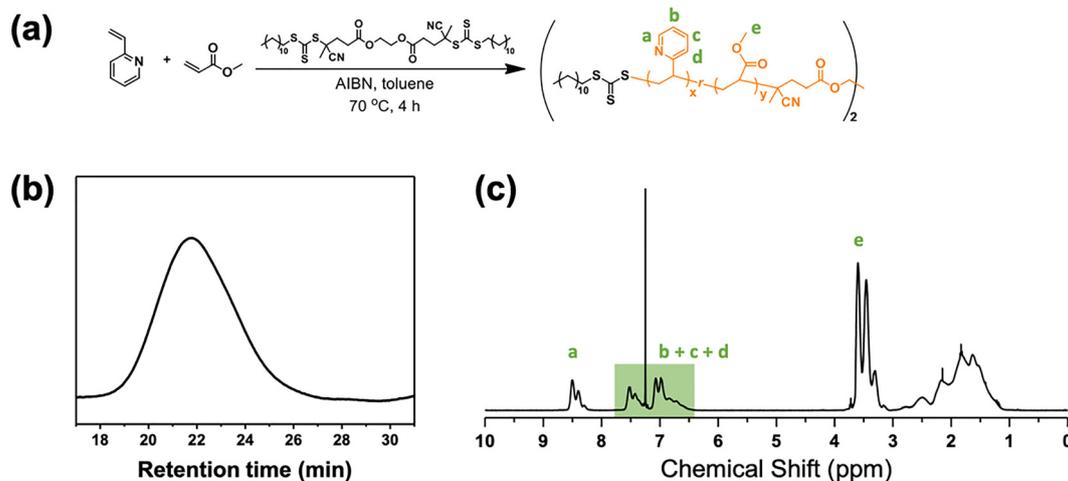
Fig. 3 (a) RAFT polymerization scheme, (b) SEC trace, and (c) ^{1}H NMR spectrum of representative poly(2VP-r-MA) sample (PVM-87k).
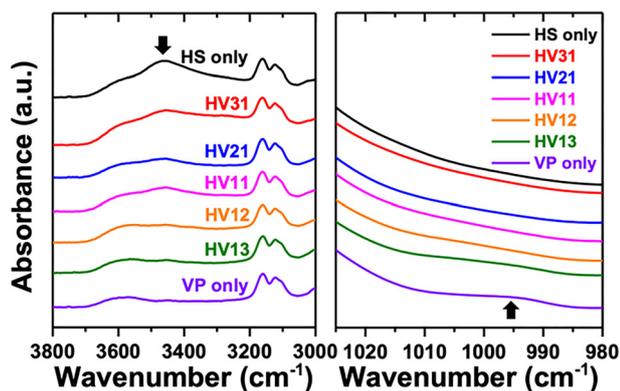

Fig. 4 ATR-FTIR spectra of the fabricated ionogels with varying weight ratios of PSHMS to PVM.

3.3. Mechanical, electrical, and adhesive properties of fabricated ionogels

The resulting freestanding ionogels were evaluated for their mechanical and electrical properties. A tensile test was first conducted on ionogels formed using PSHMS with varied M_n in the range of 85–136 kg mol^{-1} and PVM-87k at a 1:1 weight ratio of PSHMS to PVM (HV11) (Fig. 5a–c). In general, the ionogel fabricated with PSHMS of high M_n exhibited high stress at break, with a strain at break of approximately 1000% (Fig. 5a). The ionogel formed with PSHMS-114k and PVM-87k showed the highest toughness and Young's modulus, measured at 1828 kJ m^{-3} and 241 kPa, respectively (Fig. 5b). The stress at break for the ionogels ranged from 100 to 300 kPa (Fig. 5c), indicating that they are sufficiently robust for use in strain-sensor applications.[6,35–42] The stress at break, toughness, and Young's modulus tend to increase with the chain length of PSHMS, likely due to the greater number of hydrogen bonds per chain and the increased chain length available for interaction with PVM chains.[26] The average ion conductivity of the ionogels was measured to be 0.3–0.5 mS cm^{-1}, showing a trend similar to that of the mechanical properties, although the

trend remains uncertain due to substantial overlap in the error bars (Fig. 5c). Next, the effect of the M_n of PVM on the physical properties of ionogels formed with PSHMS-114k at a 1:1 weight ratio (HV11) was examined (Fig. 5d). As the M_n of PVM increased, both the toughness and stress at break varied, with the maximum stress and modulus observed at 87 kg mol^{-1} (Fig. 5e and f). Increasing the PVM chain length results in greater chain entanglement, a higher number of pyridinyl units per chain, and reduced compatibility, which are critical for effective interpenetration of the PVM chains into the assembled BCP network. Although it is challenging to deconvolute the collective influence of these individual factors in such a complex dual-polymeric crosslinking system, it is well established that mechanical properties can be significantly tuned by optimizing both composition and molecular weight to maximize specific performance characteristics.[43,44] In the present case, at M_n of 87 kg mol^{-1}, these competing factors appear to be well balanced, leading to an optimal crosslinking state and, consequently, robust mechanical properties. Similar to the variation observed with M_n of PSHMS, the average ion conductivity remained again in the range of 0.3–0.5 mS cm^{-1} (Fig. 5f). In this set of experiments, the highest toughness and Young's modulus were observed to be 2696 kJ m^{-3} and 241 kPa, respectively. Lastly, the weight ratio of PSHMS-114k to PVM-87k was varied as 3:1, 2:1, 1:1, 1:2, and 1:3, denoted as HV31, HV21, HV11, HV12, and HV13, respectively (Fig. 5g). The HV11 ionogel exhibited the highest stress at break, toughness, and Young's modulus, suggesting that the balance between hydrogen-bondable phenol and pyridine groups was optimized at this composition, maximizing its physical properties (Fig. 5h–i). Ion conductivity decreased with increasing PVM content, strongly indicating that the poly(HS-r-MA) block of PSHMS primarily governs ionic conduction.

The adhesive characteristics of the HV11 ionogel on various materials were evaluated by measuring average shear stress using a UTM, in which the film made from the material of interest was pulled in the horizontal direction. The HV11 ionogel adhered strongly to a range of materials, including
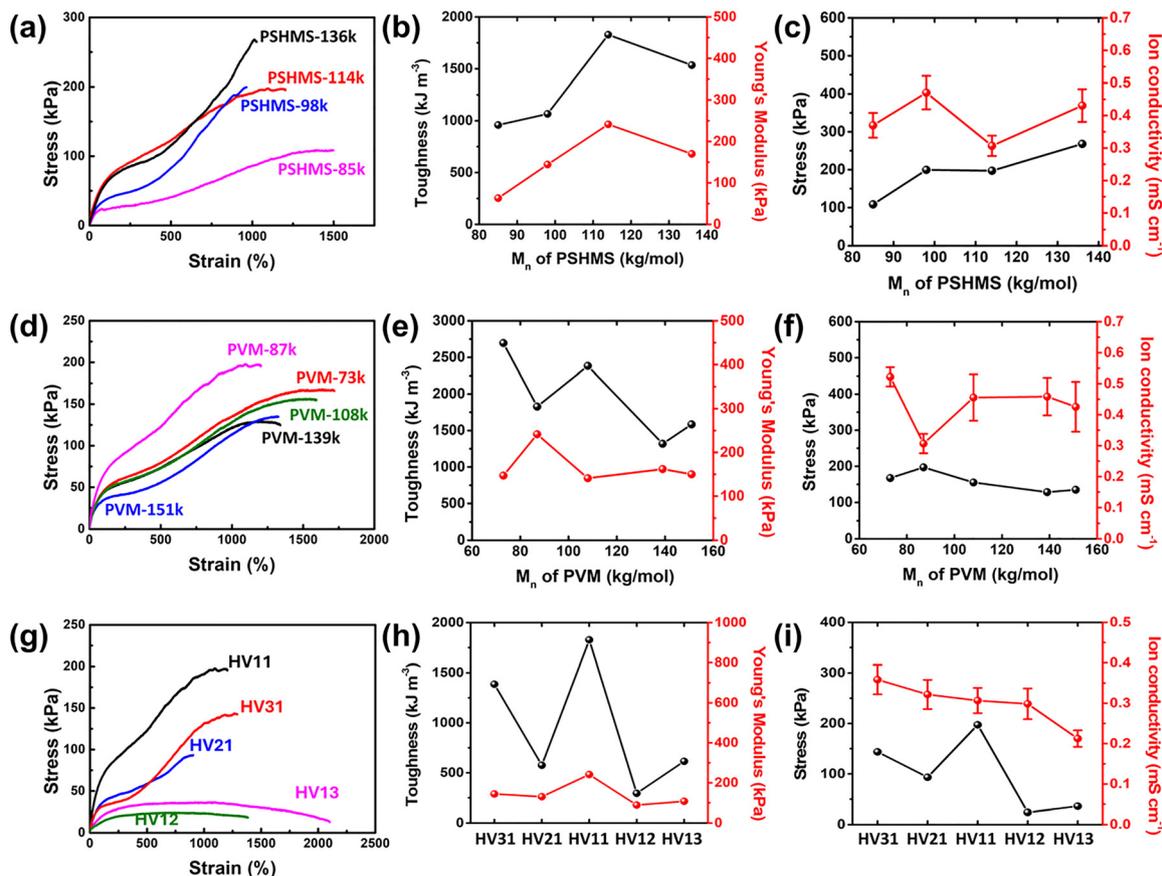
Fig. 5 (a, d and g) Stress–strain curves, (b, e and h) extracted toughness and Young's modulus, and (c, f and i) stress at break and ion conductivity of the ionogels as a function of M_n of PSHMS at fixed M_n of PVM (87.0 kg mol^{-1}) (a–c), as a function of M_n of PVM at fixed M_n of PSHMS (114 kg mol^{-1}) (d–f), and as a function of the weight ratio between PSHMS-114k and PVM-87k (g–i).

aluminum, poly(ethylene terephthalate) (PET), polyethylene (PE), polyimide (PI), poly(vinyl chloride) (PVC), poly(methyl methacrylate) (PMMA), Ecoflex, and polydimethylsiloxane (PDMS). As a reference, the average shear stress of 3 M double-sided tape was measured at 2985 kPa. The strongest adhesion was observed with PET, which exhibited approximately 50% of the shear stress of the double-sided tape. Other relatively polar materials, such as PMMA and aluminum, showed average shear stresses close to or exceeding 1000 kPa. In contrast, nonpolar polymers such as PE and PS exhibited adhesive strengths below 1000 kPa. Hydrophobic materials like Ecoflex and PDMS demonstrated even lower adhesive strengths, under 500 kPa, indicating that adhesion depends strongly on the surface chemistry of the material. The observed adhesive behavior can be attributed to functional group interactions within the ionogel system. The phenolic OH and pyridine groups in the ionogel can interact with various surface functionalities—such as ester, amide, hydroxyl, and amine groups,[45,46] as well as with metal surfaces via Lewis acid–base interactions.[47,48] Additionally, the aromatic ring groups on the surface can interact with aromatic rings in the ionogel via π–π interactions[49,50] Although the ionogel exhibits relatively weak adhesion to hydrophobic materials, it has been shown that the

HV11 ionogel can effectively adhere to such surfaces through interactions with surface-induced dipoles in the hydrophobic materials.[51,52] To impart adhesive properties to ionogels, functional monomers that promote adhesion are generally copolymerized with other comonomers in the presence of an ionic liquid and a crosslinker, resulting in the typical adhesion strength in range of 100–2000 kPa.[53] In contrast, adhesive ionogels based on BCP systems are rarely reported. A recent study described a system fabricated by mixing two block copolymers, namely poly(tert-butyl styrene-b-(hydroxystyrene-r-methyl acrylate)) and poly(tert-butyl styrene-b-(2-vinyl pyridine-r-methyl acrylate)), which exhibited moderate adhesion strengths of 15–70 kPa on various substrates.[22] Notably, the two block copolymers co-assemble into a single micellar cluster, where many functional groups in the corona region interact with their counterparts, leaving few unbound functionalities available. As a result, accessible hydrogen-bonding motifs are limited. In contrast, the design of the present system provides available functional units capable of hydrogen bonding, thereby enhancing the adhesion strength to levels comparable to those of previously reported adhesive ionogel materials.[53] Fig. 6c demonstrates the effective adhesion of the HV11 ionogel to a variety of surfaces. A 0.5 kg stainless steel counterweight
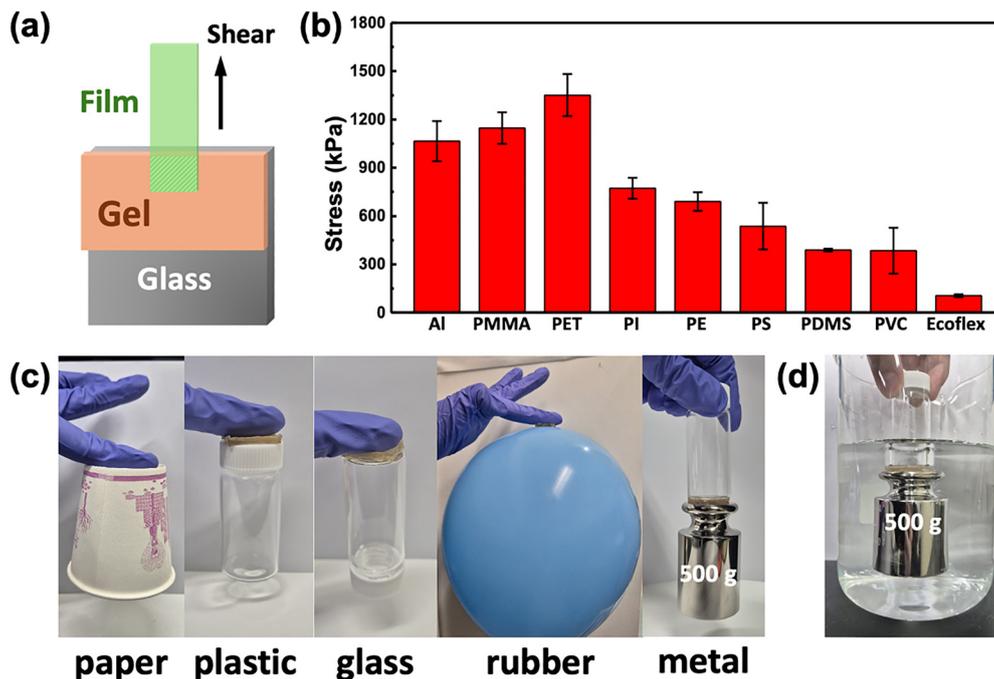
Fig. 6 (a) Schematic illustration of the adhesion test (contact dimension = 5 mm × 5 mm), and (b) average shear stress of the HV11 ionogel with different materials, obtained by pulling the material (film) of interest from the ionogel in the horizontal directions, (c) photographs displaying the strong adhesion of HV11 ionogel between a nitrile glove and different surfaces, *i.e.* paper (disposable cup), plastic (vial cap), glass (vial), rubber (balloon), and metal (0.5 kg), and (d) photograph showing underwater adhesion of HV11 ionogel between glass and metal (0.5 kg).

was not only lifted under ambient conditions but also maintained its adhesive properties under water (Fig. 6d). These observations also suggest that the adhesion of the ionogel to other materials is not significantly affected by surrounding water molecules, which is nontrivial in the field of hydrogels and ionogels.

3.4. Self-healing properties of the fabricated ionogels

The self-healing capability of the HV11 ionogel was evaluated by comparing the stress–strain curves of pristine and healed samples. The ionogel was cut into two pieces, reattached, and thermally annealed at 50 °C for 36–60 h. All ionogels composed of PSHMS polymers with varying molecular weights exhibited self-healing behavior. Fig. 7 shows the stress–strain curves of the pristine and self-healed ionogels. In all cases, the molecular weight of PSHMS ranged from 85 to 136 kg mol^{-1}, while the M_n of the PVM random copolymer was fixed at 87 kg mol^{-1}. Longer annealing times (60 h at 50 °C) enabled full recovery of the stress–strain curves to those of the pristine samples. The self-healing performance was quantified using healing efficiency (η), defined as the ratio of the stress at break, strain at break, or toughness of the healed sample to that of the pristine ionogel. The calculated η values are presented in Table S3. The HV11 ionogel fabricated with PSHMS-114k and PVM-87k exhibited the highest healing efficiencies: 96.5% (stress at break), 92.8% (strain at break), and 87.4% (toughness). A SI Movie demonstrates the stretchability of the healed ionogel, in which the interface between the rejoined segments is barely visible after healing, and the ionogel can be manually stretched without noticeable fracture.

The observed self-healing behavior confirms that the non-covalent interactions, primarily hydrogen bonding, can be reversibly broken and reformed by external stimuli. Notably, the self-healing property of the ionogel system comprising of the hydroxystyrene–pyridine-based BCP ionogels has not been previously reported,[22] however, the design of this dual association ionogel system, comprising two copolymer components, enables the presence of hydrogen-bondable units essential for self-healing. Separating the pyridinyl group onto a different chain reduces the likelihood of intramicellar hydrogen bonding, thereby increasing the probability for both PSHMS and PVM chains to move freely, interact with other chains, and access more available hydrogen-bondable groups. It is noted that η tends to increase with increasing M_n: the efficiency derived from stress at break was approximately 70% for PSHMS with an M_n of 85.5 kg mol^{-1}, increasing to over 95% at an M_n of 114 kg mol^{-1}. As external stimuli induce reversible hydrogen bond dissociation and reformation, chain mobility is enhanced. Under these conditions, longer chains are more likely to interact with other chains. When two cut pieces are reattached, this dynamic process is activated, resulting in observable self-healing behavior with a clear molecular-weight dependence.

Finally, a BCP system that does not contain HS units was synthesized and utilized for the fabrication of ionogel. RAFT polymerizations of methyl acrylate was carried out using CTA-EG, followed by chain extension with *tert*-butyl styrene *via* secondary RAFT polymerization (see SI for details of the synthesis) to produce poly(*tert*-butyl styrene-*b*-methyl acrylate-*b*-*tert*-butyl styrene) (PSMS; M_n = 72.4 kg mol^{-1}, $Đ$ = 1.35, DP_{tBS} = 65,
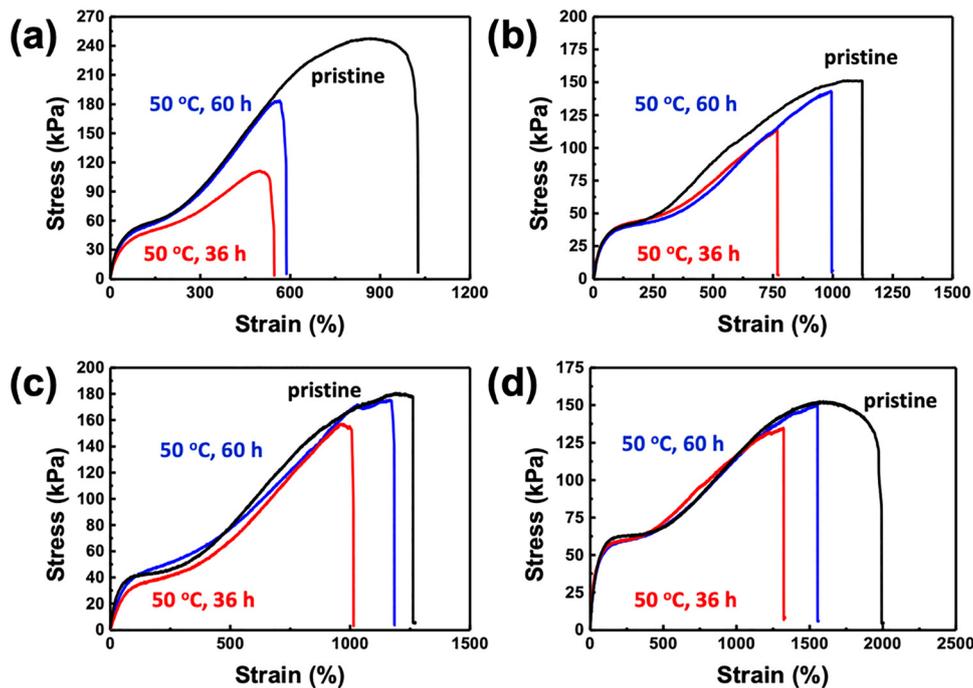
Fig. 7 Strain–stress curves of the pristine (black) and self-healed ionogels fabricated with (a) PSHMS-85k, (b) PSHMS-98k, (c) PSHMS-114k, (d) PSHMS-136k and PVM-87k by thermal annealing at 50 °C for 36 h (red), and 60 h (blue).

$DP_{MA} = 708$, $F_{MA} = 0.948$) (Fig. S4). The resulting sample was utillized to fabricate ionogel under identical processing conditions as those used for PSHMS. However, the ionogel derived from PSMS did not exhibit sufficient mechanical robustness, freestanding capability, and strong adhesiveness (Fig. S5a). Furthermore, the ionogel was deformed readily when the sample was annealed at 50 °C (Fig. S5b). These observations confirm that the freestanding capability, adhesion, and self-healing properties observed in the systems with PSHMS originate from the chemical design that providing accessible hydrogen bonding motifs within the network.

3.5. Assessment of the performance of a strain sensor

The relative resistance $(\Delta R/R_0)$ of the stretchable and self-healable ionogel sensor increases linearly with applied strain from 10% to 100%, exhibiting excellent linearity ($R^2 = 0.99$), as
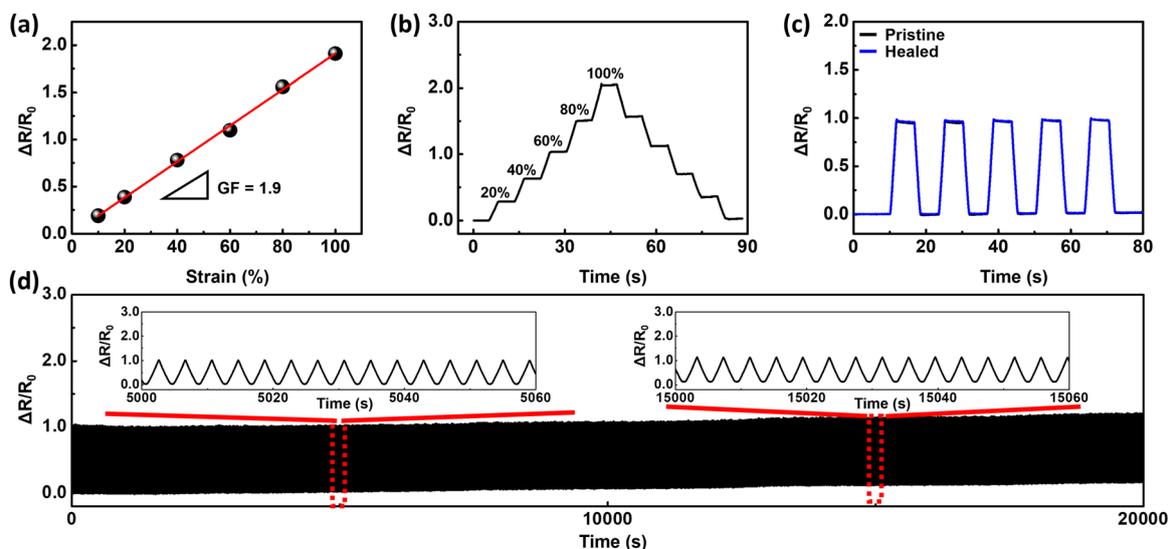
Fig. 8 (a) $\Delta R/R_0$ of the stretchable ionogel sensor under applied strains from 0% to 100%, showing a gauge factor (GF) of 1.9 and excellent linearity ($R^2 = 0.99$). (b) Stepwise $\Delta R/R_0$ responses of the strain sensor under sequential strain increments and decrements of 20% over a strain range from 0% to 100%. (c) $\Delta R/R_0$ of the pristine and self-healed ionogel sensors at 50% strain after complete cutting and subsequent self-healing. (d) Cyclic stability of the ionogel sensor under a constant strain of 50% over 20 000 s, demonstrating reliable long-term sensing performance.

shown in Fig. 8a. The calculated gauge factor (GF) of 1.9 indicates a sensitive and reproducible strain-dependent electrical response, confirming efficient transduction of mechanical deformation into an electrical signal within the ionogel. As shown in Fig. 8b, the ionogel sensor exhibits a stepwise $\Delta R/R_0$ response to tensile strain, increasing from 0% to 100% in 20% increments and then decreasing back to 0% in 20% decrements. The sensor rapidly recovers $\Delta R/R_0$ values corresponding to each strain level during both stretching and releasing processes, without noticeable hysteresis, indicating highly reversible and stable sensing behavior under repeated mechanical deformation. The ionogel developed in this work also demonstrates intrinsic self-healing capability, offering a distinct advantage for stretchable strain sensor applications by enabling reliable recovery of sensing performance after mechanical damage. As shown in Fig. 8c, the $\Delta R/R_0$ profiles of the pristine (black) and self-healed (blue) ionogel sensors under 50% strain overlap exactly, with both exhibiting consistent and repeatable responses during cyclic deformation. These results confirm the effective restoration of conductive pathways and mechanical integrity in the ionogel, underscoring its exceptional self-healing capability. Fig. 8d demonstrates the long-term operational stability of the ionogel sensor, in which $\Delta R/R_0$ was monitored during cyclic application of a constant tensile strain of 50%. The sensor exhibits stable temporal characteristics, with negligible variation in $\Delta R/R_0$ over 20 000 s, indicating excellent durability and reversibility under prolonged mechanical loading. The inset plots show that the sensor maintains consistent signal amplitude and waveform during repeated stretching–releasing cycles at approximately 5000 s and 15 000 s. Collectively, these results confirm the mechanical robustness and long-term signal stability of the ionogel-based sensor, demonstrating the suitability of the self-healable, stretchable ionogel as a reliable platform for soft-sensing applications.

4. Conclusion

In this study, we demonstrated the design of a polymeric material system enabling stretchable, mechanically robust, highly adhesive, and self-healable ionogels suitable for strain-sensor applications. The associative network within the IL was formed by two copolymeric components: a PSHMS triblock copolymer and a PVM random copolymer. The IL-phobic P*t*BS block of PSHMS forms the micellar core, while the middle block not only forms the corona structure but also bridges the micellar clusters. Additionally, pyridine groups in the PVM copolymer interact with phenol groups in the middle block of PSHMS, increasing the crosslinking density of the associative network. Both copolymers were successfully synthesized *via* sequential and random copolymerizations using a bifunctional RAFT agent. The resulting system produced freestanding ionogels with outstanding mechanical performance, exhibiting a maximum strain at break of $\approx 1000\%$, toughness of ≈ 2700 kJ m^{-3}, Young's modulus of ≈ 250 kPa, and a reasonably high ionic

conductivity of 0.3–0.5 mS cm^{-1}. We further explored the dependence of molecular weight and the weight ratio of the two copolymers on the final properties of the ionogels. At a 1 : 1 weight ratio (HV11), the stress at break, toughness, and Young's modulus increased with increasing M_n of PSHMS. In case of PVM, M_n of 87 kg mol^{-1} was found to form an optimal cross-linking state for robust mechnical properties. In addition, it was found that Young's modulus is primarily governed by the PSHMS. The optimum weight ratio was determined to be 1 : 1 (HV11), indicating that the balance between phenol and pyridine is optimal at this ratio. The HV11 ionogel exhibited strong adhesion to a wide range of materials, including plastics (PET, PE, PVC, PI, PS, and PMMA), hydrophobic elastomers (PDMS and Ecoflex), metals (aluminum and stainless steel), paper, and glass, with a maximum shear stress of ≈ 1300 kPa— approximately 50% of that of commercial double-sided tape. Furthermore, the adhesion remained effective even under water, making this ionogel platform suitable for underwater electronics. The ionogel was self-healable at 50 °C, with a healing efficiency exceeding 95%, confirming that the polymer design imparts the desired properties for high-performance strain sensors. A strain sensor fabricated using the HV11 exhibited a highly linear and reversible strain–resistance response (GF = 1.9) across a 10–100% strain range, with negligible hysteresis, rapid recovery, and stable performance under cyclic loading. Furthermore, the sensor demonstrated outstanding self-healability and long-term durability, fully restoring its electrical response post-damage and maintaining reliable $\Delta R/R_0$ signals under 50% strain for over 20 000 s. The current strategy to simultaneously impart stretchability, robustness, durability, adhesion to various substrates under ambient and aqueous conditions, and ionic conductivity into polymeric gel materials can open up a potential towards a functional material platform for wearable electronics, soft sensors, and other bio-integrated devices.

Author contributions

The manuscript was written based on contributions from all authors. All authors have given approval to the final version of the manuscript.

Conflicts of interest

There are no conflicts to declare.

Data availability

All relevant data supporting the findings of this study are available within the main text or the supplementary information (SI) which includes additional NMR spectra and SEC traces of synthesized copolymers, details for synthesis, healing efficiencies, and movie showing stretchability of the ionogel. Supplementary information: supplementary figures, table and movie. See DOI: https://doi.org/10.1039/d6tc00261g.

Acknowledgements

Notes and references

1 C. Tan, Z. Dong, Y. Li, H. Zhao, X. Huang, Z. Zhou, J.-W. Jiang, Y.-Z. Long, P. Jiang and T.-Y. Zhang, *Nat. Commun.*, 2020, **11**, 3530.

2 L. Tang, S. Wu, J. Qu, L. Gong and J. Tang, *Materials*, 2020, **13**, 3947.

3 M. Amjadi, Y. J. Yoon and I. Park, *Nanotechnology*, 2015, **26**, 375501.

4 J. Chen, J. Zheng, Q. Gao, J. Zhang, J. Zhang, O. M. Omisore, L. Wang and H. Li, *Appl. Sci.*, 2018, **8**, 345.

5 L. Xu, Z. Huang, Z. Deng, Z. Du, T. L. Sun, Z. H. Guo and K. Yue, *Adv. Mater.*, 2021, **33**, 2105306.

6 L. M. Zhang, Y. He, S. Cheng, H. Sheng, K. Dai, W. J. Zheng, M. X. Wang, Z. S. Chen, Y. M. Chen and Z. Suo, *Small*, 2019, **15**, 1804651.

7 M. Harun-Ur-Rashid, T. Foyez and A. B. Imran, *Sensors for Stretchable Electronics in Nanotechnology*, CRC Press, 2021, pp. 63–78.

8 C. Pang, G.-Y. Lee, T.-I. Kim, S. M. Kim, H. N. Kim, S.-H. Ahn and K.-Y. Suh, *Nat. Mater.*, 2012, **11**, 795–801.

9 Z. Bei, Y. Chen, S. Li, Z. Zhu, J. Xiong, R. He, C. Zhu, Y. Cao and Z. Qian, *Chem. Eng. J.*, 2023, **451**, 138675.

10 S. Xia, S. Song, F. Jia and G. Gao, *J. Mater. Chem. B*, 2019, **7**, 4638–4648.

11 S. Ryu, P. Lee, J. B. Chou, R. Xu, R. Zhao, A. J. Hart and S.-G. Kim, *ACS Nano*, 2015, **9**, 5929–5936.

12 J. Yin, S. Pan, L. Wu, L. Tan, D. Chen, S. Huang, Y. Zhang and P. He, *J. Mater. Chem. C*, 2020, **8**, 17349–17364.

13 Y. Lu, Z. Liu, H. Yan, Q. Peng, R. Wang, M. E. Barkey, J.-W. Jeon and E. K. Wujcik, *ACS Appl. Mater. Interfaces*, 2019, **11**, 20453–20464.

14 K. H. Lee, M. S. Kang, S. Zhang, Y. Gu, T. P. Lodge and C. D. Frisbie, *Adv. Mater.*, 2012, **24**, 4457–4462.

15 J. Liu, H. Song, Z. Wang, J. Zhang, J. Zhang and X. Ba, *J. Mater. Sci.*, 2020, **55**, 3991–4004.

16 S. Li, X. Zhou, Y. Dong and J. Li, *Macromol. Rapid Commun.*, 2020, **41**, 2000444.

17 K. G. Cho, Y. K. Kwon, S. S. Jang, K. H. Seol, J. H. Park, K. Hong and K. H. Lee, *J. Mater. Chem. C*, 2020, **8**, 3639–3645.

18 J. Sun, G. Lu, J. Zhou, Y. Yuan, X. Zhu and J. Nie, *ACS Appl. Mater. Interfaces*, 2020, **12**, 14272–14279.

19 R. Tamate, K. Hashimoto, T. Horii, M. Hirasawa, X. Li, M. Shibayama and M. Watanabe, *Adv. Mater.*, 2018, **30**, 1802792.

20 S. Zhang, K. H. Lee, C. D. Frisbie and T. P. Lodge, *Macromolecules*, 2011, **44**, 940–949.

21 Z. Jia, X. Xu, Q. Fu and J. Huang, *J. Polym. Sci., Part A: Polym. Chem.*, 2006, **44**, 6071–6082.

22 K. G. Cho, S. An, D. H. Cho, J. H. Kim, J. Nam, M. Kim and K. H. Lee, *Adv. Funct. Mater.*, 2021, **31**, 2102386.

23 R. Chang, H. An, X. Li, R. Zhou, J. Qin, Y. Tian and K. Deng, *Polym. Chem.*, 2017, **8**, 1263–1271.

24 S. Banerjee, B. V. Tawade and B. Améduri, *Polym. Chem.*, 2019, **10**, 1993–1997.

25 D. H. Cho, K. G. Cho, S. An, H. W. Oh, J. Yeo, W. C. Yoo, K. Hong, M. Kim and K. H. Lee, *Energy Storage Mater.*, 2022, **45**, 323–331.

26 S. Kim, S. Park, M. S. Kim, H. Lee, H. Lee, K. H. Lee and M. Kim, *ACS Appl. Mater. Interfaces*, 2024, **38**, 51459–51468.

27 Y. Zhao, F. Wang, J. Liu, D. Gan, B. Lei, J. Shao, W. Wang, Q. Wang and X. Dong, *ACS Appl. Mater. Interfaces*, 2023, **15**, 28664–28674.

28 J. Wu, L. Huang, S. Wang, X. Li, L. Wen, X. Li, T. Feng, P. Li, Z. Fang, M. Wu and W. Lv, *Energy Storage Mater.*, 2023, **57**, 549–556.

29 D. P. Sweat, X. Yu, M. Kim and P. Gopalan, *J. Polym. Sci., Part A: Polym. Chem.*, 2014, **52**, 1458–1468.

30 J. Kwak, S. H. Han, H. C. Moon, J. K. Kim, V. Pryamitsyn and V. Ganesan, *Macromolecules*, 2015, **48**, 6347–6352.

31 J. P. Gaspard, S. Creutz, P. Bouchat, R. Jerome and M. C. Stuart, *Phys. B*, 1997, **234**, 268–270.

32 S.-C. Tsai, Y.-C. Lin, E.-L. Lin, Y.-W. Chiang and S.-W. Kuo, *Polym. Chem.*, 2016, **7**, 2395–2409.

33 A. Noro, Y. Matsushita and T. P. Lodge, *Macromolecules*, 2008, **41**, 5839–5844.

34 T. Asari, S. Matsuo, A. Takano and Y. Matsushita, *Polym. J.*, 2006, **38**, 258–263.

35 Y. Zhang, J. Xu and H. Wang, *RSC Adv.*, 2021, **11**, 37661–37666.

36 X. He, W. Shi, N. Sun, M. Hou, Z. Tan, H. Jia and X. Lu, *ACS Appl. Polym. Mater.*, 2022, **4**, 6916–6924.

37 Q. Jin, L. Pan, Y. Wang, Z. Zhou and M. Zhu, *ACS Appl. Polym. Mater.*, 2024, **6**, 4798–4807.

38 L. Sun, H. Huang, Q. Ding, Y. Guo, W. Sun, Z. Wu, M. Qin, Q. Guan and Z. You, *Adv. Fiber Mater.*, 2022, **4**, 98–107.

39 Z. Jin, L. An and H. Zhang, *ACS Appl. Polym. Mater.*, 2023, **5**, 2704–2715.

40 J. Lai, H. Zhou, Z. Jin, S. Li, H. Liu, X. Jin, C. Luo, A. Ma and W. Chen, *ACS Appl. Mater. Interfaces*, 2019, **11**, 26412–26420.

41 L. Sun, S. Chen, Y. Guo, J. Song, L. Zhang, L. Xiao, Q. Guan and Z. You, *Nano Energy*, 2019, **63**, 103847.

42 P. Shi, Y. Wang, W. W. Tjiu, C. Zhang and T. Liu, *ACS Appl. Mater. Interfaces*, 2021, **13**, 49358–49368.

43 D. Son, H. Hwang, J. F. Fontenot, C. Lee, J. P. Jung and M. Kim, *ACS Omega*, 2022, 7, 30028–30039.

44 S. Pruksawan, J. W. R. Lim, Y. L. Lee, Z. Lin, H. L. Chee, Y. T. Chong, H. Chi and F. Wang, *Commun. Mater.*, 2023, **4**, 75.

45 S. Malynych, I. Luzinov and G. Chumanov, *J. Phys. Chem. B*, 2002, **106**, 1280–1285.

46 S. Wang, Y. Fang, H. He, L. Zhang, C. A. Li and J. Ouyang, *Adv. Funct. Mater.*, 2021, **31**, 2007495.

47 D. H. Kim, K. H. Kim, W. H. Jo and J. Kim, *Macromol. Chem. Phys.*, 2000, **201**, 2699–2704.

48 D. Mollenhauer, N. Gaston, E. Voloshina and B. Paulus, *J. Phys. Chem. C*, 2013, **117**, 4470–4479.

49 E. Y. Jeon, B. H. Hwang, Y. J. Yang, B. J. Kim, B.-H. Choi, G. Y. Jung and H. J. Cha, *Biomaterials*, 2015, **67**, 11–19.

50 Q. Lu, D. X. Oh, Y. Lee, Y. Jho, D. S. Hwang and H. Zeng, *Angew. Chem., Int. Ed.*, 2013, **125**, 4036–4040.

51 Q. Lu, E. Danner, J. H. Waite, J. N. Israelachvili, H. Zeng and D. S. Hwang, *J. R. Soc., Interface*, 2013, **10**, 20120759.

52 J. Yu, Y. Kan, M. Rapp, E. Danner, W. Wei, S. Das, D. R. Miller, Y. Chen, J. H. Waite and J. N. Israelachvili, *Proc. Natl. Acad. Sci. U. S. A.*, 2013, **110**, 15680–15685.

53 Y. Huang, H. Zhu, Q. Zhang and S. Zhu, *Macromol. Rapid Commun.*, 2025, **46**, 2400973.